SLAC-PUB-15933
IPPP-14-23
DCP-14-46
MCNET-14-007
ZU-TH 13/14

Triple vector boson production through Higgs-Strahlung with NLO multijet merging

S. Höche[1], F. Krauss[2], S. Pozzorini[3], M. Schönherr[2], J. M. Thompson[2], K. C. Zapp[4]

[1] SLAC National Accelerator Laboratory, Menlo Park, CA 94025, USA
[2] Institute for Particle Physics Phenomenology, Durham University, Durham DH1 3LE, UK
[3] Physik–Institut, Universität Zürich, CH–8057 Zürich, Switzerland
[4] CERN, Department of Physics, CH-1211 Geneva 23, Switzerland

Abstract: Triple gauge boson hadroproduction, in particular the production of three W-bosons at the LHC, is considered at next-to leading order accuracy in QCD. The NLO matrix elements are combined with parton showers. Multijet merging is invoked such that NLO matrix elements with one additional jet are also included. The studies here incorporate both the signal and all relevant backgrounds for VH production with the subsequent decay of the Higgs boson into $W-$ or $\tau-$-pairs. They have been performed using Sherpa+OpenLoops in combination with Collier.

1 Introduction

With the imminent second round of data taking at the LHC, at higher energies than ever before and with more events to analyze, new opportunities present themselves for studying physics at the electroweak to TeV scale. In light of the recent discovery of a Higgs boson [1, 2], with all experimental determinations of its properties up to now compatible with Standard Model expectations based on the Brout–Englert–Higgs (BEH) mechanism [3–6], it is clear that increasingly precise studies become necessary in order to look for subtle effects where new physics could manifest itself.

A prime candidate for such studies is the production of multiple gauge bosons: channels involving ZZ, WW and $\gamma\gamma$ final states have been employed, among others, for the discovery of the Higgs boson, while processes with $W\gamma$, WZ, ZZ, and $Z\gamma$ final states are frequently used by the experiments to search for anomalous triple gauge boson couplings, see for instance [7–10]. Clearly, with higher energies, such searches can and will be extended to also include anomalous quartic gauge couplings. In addition, multi-boson channels, and in particular those that lead to final states involving three leptons, are important backgrounds in searches for new particles; as illustrative example consider neutralino-chargino pair production and their subsequent decay in supersymmetric extensions of the Standard Model.

This publication focuses on the production of a Standard Model Higgs boson in the Higgsstrahlung process (associated VH production) and its subsequent decay into $W-$ or $\tau-$pairs. Apart from the signal, all relevant background channels will be studied as well. This includes multiple gauge bosons final states such as WZ,

WWW, ZWW, ZZ, WZZ and ZZZ. The studies presented here follow closely the recent analyses by ATLAS and CMS [11, 12].

In many of these processes, QCD corrections play a significant role, from highly phase-space dependent K-factors ranging between 1.5 and 2 to the fact that the emergence of additional jets can be used to shed light on the actual production mechanism giving rise to triple gauge boson final states. In addition, quite often vetoing additional jets is a very good way to suppress unwanted backgrounds, a prime example being the massive suppression of the $t_{\to W^+b}\bar{t}_{\to W^-\bar{b}}W$ background to WWW production or other signals, which allows us here to ignore this class of processes.

For the signal process, VH–associated production, parton–level results are available at next-to leading order accuracy (NLO) in the perturbative expansion of QCD [13] and NNLO are results are known for more than a decade [14, 15]. The NLO QCD corrections to triple gauge boson production have first been calculated in [16, 17], the leptonic decay of the bosons has been discussed in [18, 19] and it has also been implemented in the VBFNLO code [20]. Predictions at NLO QCD for triple gauge boson production in association with one extra jet are presented for the first time in this paper.

For the calculation of the virtual corrections we employ OPENLOOPS [21], a fully automated one-loop generator based on a fast numerical recursion for multi-particle processes. For tensor and scalar integrals we use the COLLIER library [22], which guarantees high numerical stability thanks to the methods of [23–25]. For the Born and real emission contributions the matrix element generators AMEGIC++ [26] and COMIX [27] are used. The mutual cancellation of infrared divergences in real and virtual contributions is achieved through the dipole formalism [28, 29] and its automated implementation in both AMEGIC++ [30] and COMIX. The overall event generation is handled by SHERPA [31, 32]. For the first time, the NLO QCD calculations are combined consistently with parton showers, employing the S–MC@NLO variant [33, 34] of MC@NLO [35, 36]. Parton showers are generated by SHERPA, based on Catani–Seymour dipole subtraction [28, 29] as suggested in [37] and implemented in [38]. This setup for the matching was recently employed for $t\bar{t}b\bar{b}$ production in [39]. In addition, a multijet merging with NLO matrix elements including one additional jet is included, following the MEPS@NLO algorithm [40, 41]. This method has recently been employed for a number of processes, among them top pair production with up to two jets [42, 43] and, similarly, the production of 4 leptons in association with up to one jet [44][1].

In the processes discussed here the treatment of hard QCD radiation is an important aspect. Corresponding aspects of the Monte-Carlo simulation are addressed in Sec. 2. In the next section, Sec. 3, results obtained with the S–MC@NLO matching to the parton shower and with the MEPS@NLO multijet merging method are presented. The focus will be on the treatment of both the signal and the backgrounds to WH associated production, with typical cuts as exemplified by the respective VH production analyses of ATLAS and CMS, [11, 12]. This publication closes with a summary and some outlook in Section 4.

2 Matching and merging techniques in SHERPA

This section reviews the basic MC event generation techniques used to produce event samples for this study. We focus on new developments in matching and merging methods, which allow to combine fixed-order NLO calculations and parton shower simulations.

2.1 S–MC@NLO

Leading order cross sections, including the subsequent parton shower evolution in the initial and final state can schematically be written as

$$\mathrm{d}\sigma^{(\mathrm{PS})} = \mathrm{d}\Phi_B \, \mathrm{B}_n(\Phi_B) \, \mathcal{F}_n(\mu_Q^2) \, . \tag{2.1}$$

In this equation, $\mathrm{d}\Phi_B$ denotes the phase space element for the Born–level kinematics and $\mathrm{B}_n(\Phi_B)$ is the Born–level differential cross section with n external partons, composed of the corresponding parton–level cross section at leading order, convoluted with the PDFs and multiplied with suitable symmetry and flux factors. The parton shower evolution of the n–parton configuration is encoded in the generating functional, $\mathcal{F}_n(t)$ with the evolution starting scale t. In principle, this scale is a free scale entering in addition to the

[1] There are, of course, other matching algorithms such as the POWHEG method described in [45, 46], and also merging algorithms, both for matrix elements at leading order [47–53] and at next-to leading order [54–56].

renormalization and factorization scales μ_R and μ_F, and it may be chosen in a process–dependent way. The parton–shower generating functional is defined by splitting kernels K_n, which convert an n–parton configuration into an $(n+1)$–parton configuration. It is given by

$$\mathcal{F}_n(t) \;=\; \Delta_n(t_c,t) \;+\; \int_{t_c}^{t} \mathrm{d}\Phi_1' \, \mathrm{K}_n(\Phi_1') \, \Delta_n(t',t) \, \mathcal{F}_{n+1}(t') \,, \tag{2.2}$$

where the Sudakov form factor $\Delta_n(t',t)$ reads

$$\Delta_n(t',t) \;=\; \exp\left[- \int_{t'}^{t} \mathrm{d}\Phi_1 \, \mathrm{K}_n(\Phi_1) \right] . \tag{2.3}$$

The phase space of the emission of the additional single parton is parametrized through the evolution parameter t, the splitting variable z, and the azimuthal angle ϕ as

$$\mathrm{d}\Phi_1 \;=\; \mathrm{d}t \, \mathrm{d}z \, \mathrm{d}\phi \, J(t,z,\phi) \,, \tag{2.4}$$

where $J(t,z,\phi)$ denotes a Jacobian factor and t_c is the infrared cut-off of the parton shower, typically of the order of a GeV. Eq. (2.2) simultaneously describes the probability of no further parton emission (first term) and a single independent emission at scale t' (second term). If such an emission takes place, Eq. (2.2) is iterated, with the boundary conditions set by the newly formed partonic state.

By now, there are two different classes of algorithms to promote the leading order (LO) expression in Eq. (2.1) to NLO accuracy, namely the POWHEG method [45,46] and the MC@NLO matching method [35]. In the latter, the usual infrared subtraction facilitating the mutual cancellation of infrared divergences between the real and virtual contributions is modified by directly using parton shower kernels, which provide a leading color approximation to the full subtraction kernels used in the fixed–order calculations. The full color correctness at fixed–order is restored by suitably chosen hard remainder terms, which compensate the difference between the full real emission contributions and the subtraction term. In [33, 34, 57] this method was extended by modifying the parton shower such that it generates its first emission with the full subtraction kernels, thereby introducing some color–suppressed but singular contributions into the Sudakov form factor. This latter method is referred to as S–MC@NLO in the following. Its cross section is computed as

$$\mathrm{d}\sigma^{(\text{S–MC@NLO})} \;=\; \mathrm{d}\Phi_B \, \bar{\mathrm{B}}_n(\Phi_B) \, \bar{\mathcal{F}}_n(\mu_Q^2) \;+\; \mathrm{d}\Phi_R \, \mathrm{H}_n(\Phi_R) \, \mathcal{F}_{n+1}(\tilde{\mu}_Q^2) \,, \tag{2.5}$$

where the combination of $\bar{\mathrm{B}}$ and H provides the exact next-to leading order cross section. H captures the MC-subtracted real-emission contribution, while $\bar{\mathrm{B}}$ contains all other terms, projected onto Born kinematics.

$$\begin{aligned} \bar{\mathrm{B}}_n(\Phi_B) \;&= \mathrm{B}_n(\Phi_B) + \tilde{\mathrm{V}}_n(\Phi_B) + \mathrm{I}_n(\Phi_B,\, \mu_Q^2) \,, \\ \mathrm{H}_n(\Phi_R) \;&= \mathrm{R}_n(\Phi_R) - \mathrm{D}_n(\Phi_R) \, \Theta\left(\mu_Q^2 - t\right) \,. \end{aligned} \tag{2.6}$$

In addition to the squared Born matrix element $\mathrm{B}_n(\Phi_B)$ the virtual and real corrections, $\tilde{\mathrm{V}}_n(\Phi_B)$ and $\mathrm{R}_n(\Phi_R)$ respectively, have been introduced, the latter together with the corresponding phase space element $\mathrm{d}\Phi_R$. This phase space element factorizes as $\Phi_R = \Phi_B \times \Phi_1$, which is used to facilitate integration of the subtraction terms $\mathrm{D}_n(\Phi_B,\Phi_1)$ over the one–particle emission phase space and arrive at the integrated subtraction terms $\mathrm{I}_n(\Phi_B)$,

$$\mathrm{I}_n(\Phi_B,\, \mu_Q^2) \;=\; \int \mathrm{d}\Phi_1 \, \mathrm{D}_n(\Phi_B,\Phi_1) \, \Theta\left(\mu_Q^2 - t\right) \,. \tag{2.7}$$

Equation (2.7) is known analytically in d dimensions for $\mu_Q^2 \to \infty$ [28, 29], as is necessary to extract the poles in the dimensional regularization parameter ε. The value for finite μ_Q^2 is computed by calculating the finite remainder in $d = 4$ dimensions with Monte-Carlo techniques [33, 34, 57].

The factorization of the full real–emission phase space is also essential to make a connection with the parton shower. In the parton shower, the one–emission phase space is bounded from above by the resummation scale μ_Q, which is suitably defined in terms of the evolution parameter t. The generating functional of the first emission in the matched calculation is

$$\bar{\mathcal{F}}_n(t) \;=\; \bar{\Delta}_n(t_c,t) \;+\; \int_{t_c}^{t} \mathrm{d}\Phi_1' \, \frac{\mathrm{D}_n(\Phi_B,\Phi_1')}{\mathrm{B}_n(\Phi_B)} \, \bar{\Delta}_n(t',t) \, \mathcal{F}_{n+1}(t') \,. \tag{2.8}$$

Its splitting kernels are given by $\mathrm{D}(\Phi_B,\Phi_1')/\mathrm{B}(\Phi_B)$ while its Sudakov factor is denoted $\bar{\Delta}(t',t)$. This expression differs from Eq. (2.2) only through sub-leading color terms and spin correlation effects. Note that all subsequent emissions after the first are treated by a standard parton shower, as indicated by $\mathcal{F}_{n+1}(t')$.

2.2 MENLOPS

The method outlined above can be augmented by leading order matrix elements for higher jet multiplicities, i.e. matrix elements for $(n+2)$, $(n+3)$ etc. external particles through a multi-jet merging technique [58,59]. A merging scale $Q_{\rm cut}$ is introduced, like in the pure LO merging algorithms [47–53], which restricts the phase space of emissions in the parton shower from above, and emissions in the matrix elements from below.

The restricted MC@NLO simulation for the "core" process with n particles generates the following terms

$$\begin{aligned} \mathrm{d}\sigma_n^{\rm excl} &= \mathrm{d}\Phi_n\, \bar{\mathrm{B}}_n(\Phi_n)\, \bar{\mathcal{F}}_n(\mu_Q^2\,;<Q_{\rm cut}) \\ &\quad + \mathrm{d}\Phi_{n+1}\, \Theta(Q_{\rm cut}-Q(\Phi_{n+1}))\, \mathrm{H}_n(\Phi_{n+1})\, \mathcal{F}_{n+1}(\mu_Q^2\,;<Q_{\rm cut})\ , \end{aligned} \tag{2.9}$$

where $\bar{\mathcal{F}}_n(\mu_Q^2\,;<Q_{\rm cut})$ is the functional of the vetoed S–MC@NLO, and $\mathcal{F}_{n+1}(\mu_Q^2\,;<Q_{\rm cut})$ is the functional of the truncated vetoed parton shower [45,46,53].

The next higher jet multiplicities are calculated at leading order accuracy. A local K-factor is applied to preserve the total cross section to NLO accuracy.

$$\mathrm{d}\sigma_{n+k} = \mathrm{d}\Phi_{n+k}\, \Theta(Q(\Phi_{n+k})-Q_{\rm cut})\, k_n(\Phi_{n+1}(\Phi_{n+k}))\ \mathrm{B}_{n+k}(\Phi_{n+k})\ \mathcal{F}_{n+k}(\mu_Q^2\,;<Q_{\rm cut})\ . \tag{2.10}$$

Here $\Phi_{n+1}(\Phi_{n+k})$ is defined by the kinematics mapping of the parton shower, and

$$k_n(\Phi_{n+1}) \;=\; \frac{\bar{\mathrm{B}}_n(\Phi_n)}{\mathrm{B}_n(\Phi_n)}\left(1-\frac{\mathrm{H}_n(\Phi_{n+1})}{\mathrm{R}_n(\Phi_{n+1})}\right)+\frac{\mathrm{H}_n(\Phi_{n+1})}{\mathrm{R}_n(\Phi_{n+1})}\ . \tag{2.11}$$

is the local K-factor. It is constructed such that a sample where exactly one jet at leading order accuracy is merged on top of the underlying S–MC@NLO reproduces this S–MC@NLO except for potential sub-leading color corrections in the S–MC@NLO n-jet simulation versus the showered $n+1$-jet simulation.

2.3 MEPS@NLO

The above merging method can be extended to the next-to-leading order also for the $n+k$-jet exclusive simulations. In order not to spoil the NLO-accuracy of these simulations it is not enough to simply implement a truncated vetoed parton shower as this is done in leading-order merging. The first-order expansion of the vetoed shower would generate corrections of order α_s, which must be subtracted. This leads to the following expression for the differential cross section in the $n+k$-jet sample:

$$\begin{aligned} \mathrm{d}\sigma_{n+k}^{\rm excl} &= \mathrm{d}\Phi_{n+k}\, \Theta(Q(\Phi_{n+k})-Q_{\rm cut})\, \tilde{\mathrm{B}}_{n+k}(\Phi_n+k)\, \bar{\mathcal{F}}_{n+k}(\mu_Q^2\,;<Q_{\rm cut}) \\ &\quad + \mathrm{d}\Phi_{n+k+1}\, \Theta(Q(\Phi_{n+k})-Q_{\rm cut})\, \Theta(Q_{\rm cut}-Q(\Phi_{n+k+1}))\, \tilde{\mathrm{H}}_{n+k}(\Phi_{n+k+1})\, \mathcal{F}_{n+k+1}(\mu_Q^2\,;<Q_{\rm cut})\ , \end{aligned} \tag{2.12}$$

The extended subtraction is implemented by the modified differential cross sections $\tilde{\mathrm{B}}_{n+k}(\Phi_{n+k})$ and $\tilde{\mathrm{H}}_{n+k}(\Phi_{n+k+1})$, defined as

$$\begin{aligned} \tilde{\mathrm{B}}_i(\Phi_i) &= \mathrm{B}_i(\Phi_i)+\tilde{\mathrm{V}}_i(\Phi_i)+\mathrm{I}_i(\Phi_i)+\int \mathrm{d}\Phi_1\ \Big[\tilde{\mathrm{D}}_i(\Phi_i,\Phi_1)-\mathrm{D}_i(\Phi_i,\Phi_1)\Big] \\ \tilde{\mathrm{H}}_i(\Phi_{i+1}) &= \mathrm{R}_i(\Phi_{i+1})-\tilde{\mathrm{D}}_i(\Phi_{i+1})\ , \end{aligned} \tag{2.13}$$

which take the probability of truncated parton shower emissions into account [40,41]. To this end, the dipole terms used in the S–MC@NLO are extended by the parton-shower emission probabilities, $\mathrm{B}_i(\Phi_i)\,\mathrm{K}_j(\Phi_{1,i+1})$, where $\mathrm{K}_j(\Phi_{1,i+1})$ is the sum of all shower splitting functions for the intermediate state with $j<i$ in a predefined shower tree which leads to the final state with kinematical configuration Φ_i.

$$\tilde{\mathrm{D}}_i(\Phi_{i+1}) \;=\; \mathrm{D}_i(\Phi_{i+1})\,\Theta(t_i-t_{i+1}) \;+\sum_{j=0}^{i-1}\mathrm{B}_i(\Phi_i)\,\mathrm{K}_j(\Phi_{1,i+1})\,\Theta(t_j-t_{i+1})\,\Theta(t_{i+1}-t_{j+1})\,\Big|_{t_0=\mu_Q^2}\ . \tag{2.14}$$

This expression has a simple physical interpretation: The first term corresponds to the coherent emission of a parton from the external i-parton final state. It contains all soft and collinear singularities which are present in the real-emission matrix elements. The sum in the second term corresponds to emissions from the intermediate states with i partons and in fact the terms $\mathrm{B}_i(\Phi_i)\,\mathrm{K}_j(\Phi_{1,i+1})$ stem from the expansion of the Sudakov form factor of the truncated shower to first order in the strong coupling. All these terms can be implemented in the parton shower approximation, because soft divergences are regulated by the finite mass of the intermediate particles.

Cut	ATLAS	CMS
$p^l_{\perp,\,\mathrm{min}}$	10 GeV	10 GeV
$\lvert\eta^e_{\mathrm{max}}\rvert$	2.47	2.5
$\lvert\eta^\mu_{\mathrm{max}}\rvert$	2.5	2.4
N_{leptons}	3	$\geq$3
Z veto	no SFOS	$\lvert m_Z - m_{SFOS}\rvert > 25$GeV
|sum of lepton charge|	1	1
Jet $p_\perp$ min	25 GeV	20 GeV
Jet dR	0.4	0.5
$E^{\mathrm{miss}}_{\perp,\,\mathrm{min}}$	–	40 GeV

Table 1: Cuts for the ATLAS and CMS analyses

3 Results

3.1 Details of the analyses

There are current efforts from both CMS and ATLAS to search for the trilepton final states emerging from WH–associated production[2], where the Higgs boson decays either into τ or W pairs [11, 12]. These final states allow a direct probe of the coupling between the Higgs boson and the weak bosons. In the following we present two analyses, namely a recent one by the ATLAS collaboration [60] and the one by the CMS collaboration [12]. The majority of the cuts that are applied in both are given below in Tab. 1. In addition to a Z veto, which is realized differently in both analysis, they both exploit jet vetoes to eliminate the large background from $t\bar{t}V$ production. Jets are reconstructed in both analyses using the anti-k_T algorithm [61,62], and events are allowed to contain at most one jet, which must not be a b-jet.

In addition to Tab. 1, the ATLAS analysis also includes a trigger on the $p_\perp$ of the leptons. This requires that at least one of them has to be above the trigger threshold of $p_\perp > 25\,\mathrm{GeV}$ for electrons and $p_\perp > 21\,\mathrm{GeV}$ for muons. The leptons are labeled in the following way: the lepton with charge different from the others is called lepton 0, of the two others the one with smaller distance ΔR from lepton 0 is lepton 1 and the remaining one is label-led as lepton 2. The leptons are considered isolated if the transverse energy of all visible particles in a cone of radius $\Delta R_{\mathrm{iso}} = 0.2$ for leptons 0 and 1 and $\Delta R_{\mathrm{iso}} = 0.4$ for lepton 2 around the lepton is less than 10 % of the lepton $p_\perp$. After pre-selection events containing a same-flavor-opposite-sign (SFOS) lepton pair are classified as Z enriched, those that don't belong to the Z depleted sample. The region considered in this publication is the Z depleted region, and in this the $E^{\mathrm{miss}}_\perp$ is required to be larger than 25 GeV in the experimental analysis, however the distributions presented here are taken from before this cut is applied.

In the CMS analysis, the hardest lepton is required to have $p_\perp > 20$GeV, and all events which have a jet with $p_\perp > 40$GeV are vetoed, as are all events containing b-jets. In the CMS analysis, there is a similar process of lepton isolation as in the ATLAS case. However, in this analysis the radius for reconstruction depends on the lepton flavor. For electrons, this is $\Delta R = 0.4$ and for muons it is 0.3. For both lepton flavors, the sum of the transverse energy of all visible particles must not exceed 0.15 of the lepton $p_\perp$.

Both the ATLAS and CMS analyses include regions with more cuts than are described here, however the observables presented do not use these regions.

3.2 Monte Carlo samples

All trilepton processes that involve an on–shell Higgs boson ($W^\pm H(\to W^+W^-)$, $W^\pm H(\to \tau^+\tau^-)$ and $ZH(\to W^+W^-)$) are considered as signal processes, and those which do not are considered background processes. In addition, The production of a Higgs boson decaying to an on-shell V boson pair is considered as part of the background. The cross section for this process is very small as compared to the production of the on-shell Higgs boson, and it contributes mostly through its interference with the triple boson background.

[2] Note that the ATLAS publication also includes similar searches in ZH–associated production which will not be considered here.

Gauge boson decays are treated in the narrow width approximation, including spin correlation effects. The kinematics are then corrected by redistributing the propagator mass onto a Breit-Wigner distribution.

The background processes considered are high multiplicity bosonic final states: $W^{\pm}Z$, ZZ, $W^{\pm}W^{+}W^{-}$, $W^{+}W^{-}Z$, $W^{\pm}ZZ$ and ZZZ. Higher multiplicity final states do not have a significant enough contribution to be considered. The WZ boson background remains dominant over large portions of phase space; this is due to lost leptons and, more importantly, due to τ decays, which lead to leptons evading the Z veto.

In order to prevent $t\bar{t}V$ contributions entering the $W^{\pm}W^{+}W^{-}$ calculation in the NLO WWWj calculation, only light quarks are considered in the matrix element final state.

The distributions for the central values include hadronization and an underlying event simulation. The uncertainties in all plots below are shown as 2 bands, one for the combined background and one for the combined signal, which have been evaluated at the parton level. The hadronisation uncertainties are very small, and therefore these parton level uncertainties are used for the hadron level results. They are obtained as quadratic sums of the envelopes provided by the variation of the perturbative scales, μ_R, μ_F, and μ_Q, and the merging scale Q_{cut}:

- $\mu_{F,R}$ are the fixed order scales, the factorization and renormalization scales, defined through the matching algorithm as detailed in [41]. These are varied by a factor of 2
- μ_Q is the resummation scale, also defined in [41]. This is varied by a factor of $\sqrt{2}$
- Q_{cut} is the merging scale. Three values are chosen for this scale, 15 GeV, 30 GeV and 60 GeV.

The electroweak input paramaters for this simulation are $\alpha = 1/128.802$, $m_W = 80.419$ GeV, $m_Z = 91.188$ GeV and $m_h = 125$ GeV.

3.3 Results with MePs@Nlo

This section presents results at MePs@Nlo for the relevant backgrounds. The sub-dominant ZZ and triple gauge boson processes, $W^{+}W^{-}Z$, $W^{\pm}ZZ$ and ZZZ, are considered at NLO accuracy with leading order merged jets, i.e. with MEnloPS. All other processes, the signal processes and the dominant WZ and WWW backgrounds are considered with the MePs@Nlo method, with one additional jet calculated to NLO accuracy.

After the veto on the Z boson and final state b quarks, the invariant mass distribution of the 3 leptons can be used to distinguish the signal from the background. In Fig. 1, we use the cuts from the CMS analysis above, the findings for a similar plot using the ATLAS cuts are practically identical. The plot shows that the main signal process, $W^{\pm}H(W^{+}W^{-})$, is clearly visible in the low mass region. In the high mass tail of the distribution, the triple gauge boson processes become more significant as the $W^{\pm}H$ and WZ distributions drop off quickly, as can be seen in the inlaid logarithmic plot.

A somewhat complementary observable is the missing energy distribution, exhibited in Fig. 2, again with cuts taken from the CMS analysis. The findings indeed display a similar behavior to the trilepton mass distribution in Fig. 1, in that the signal is clearly visible above the background at the lower energy section of the plot. In both observables, the WZ background is the most dominant background.

Also for the case where the Z veto is implemented through a veto on SFOS lepton pairs, as in the ATLAS analysis, the $E_{\perp}^{\text{miss}}$ distribution clearly shows a difference between the signal and the background. This is displayed in Fig. 3. In contrast to the case of a Z veto through a mass window as in CMS, where the distribution especially for WZ falls off smoothly, here the Z veto introduces a visible kink, while the signal remains unaffected. This of course could be further used to reduce the WZ background by utilizing this different impact on the respective shapes.

The angular observables are interesting observables for this process. Fig. 4 shows the distance in ΔR between the closer pair of oppositely signed leptons, following the ATLAS analysis. These leptons do not have the same flavor, as this observable isolates the leptons that are most likely to be products of the Higgs boson decay to $W^{+}W^{-}$ or τ–pairs. This effect in particular on the WW channel stems from the spin correlations in the decay of the Higgs boson, as already discussed in [11]. As a result, this observable also has good discriminating power between signal and background.

The different uncertainties have been investigated individually for all processes to check for their dominant source. In nearly all bins of all observables considered here, the uncertainties are driven mainly by the renor-

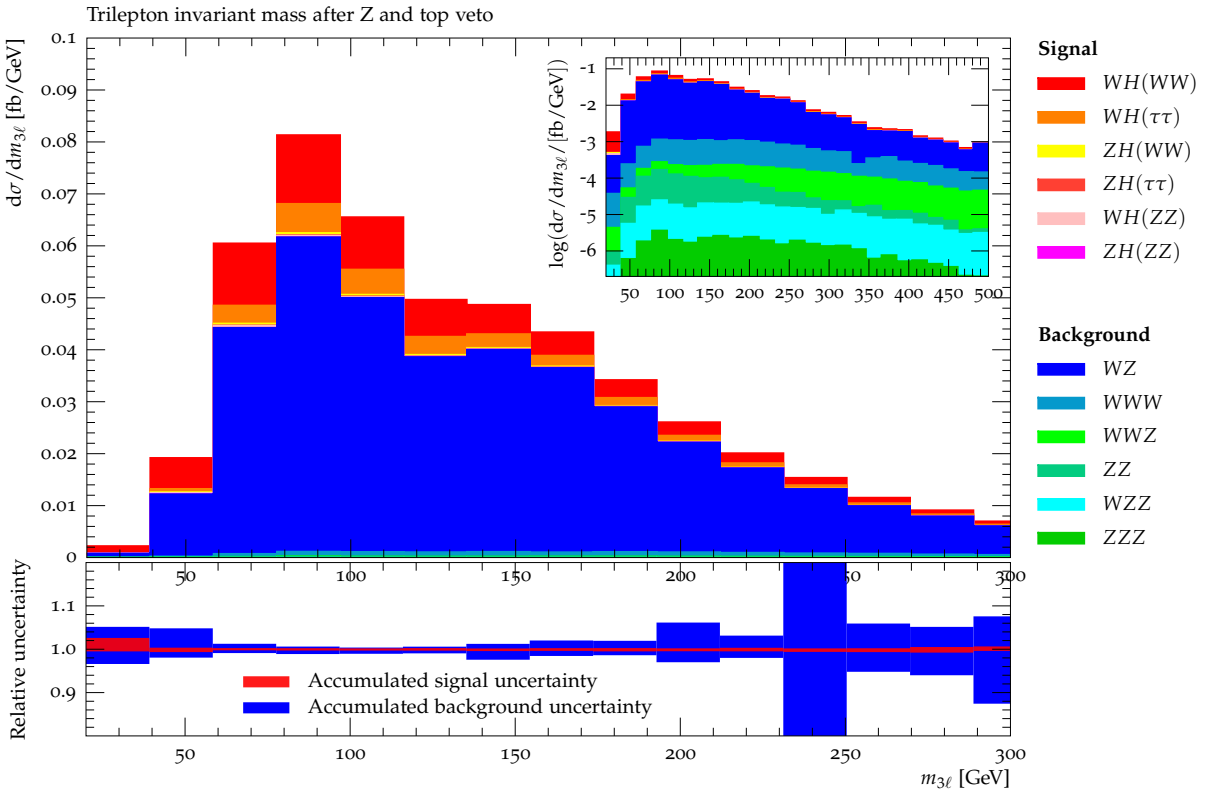

Figure 1: The trilepton invariant mass with the CMS cuts is shown to be a useful observable for discriminating signal from background in the low mass regions. This is also an observable where the triple boson production forms a significant amount of the background after the Z boson veto.

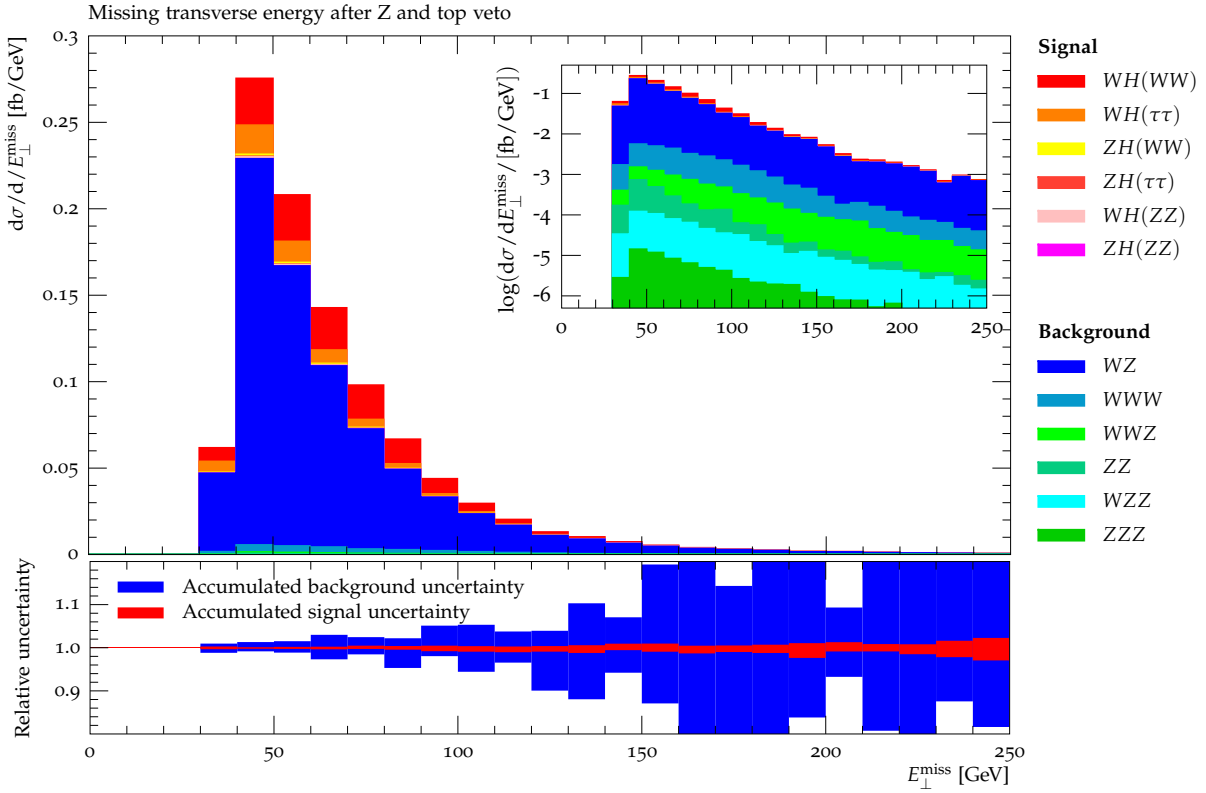

Figure 2: The $E_{\perp}^{\text{miss}}$ distribution with the CMS cuts. The distributions for signal and background in this case both have a very similar shape.

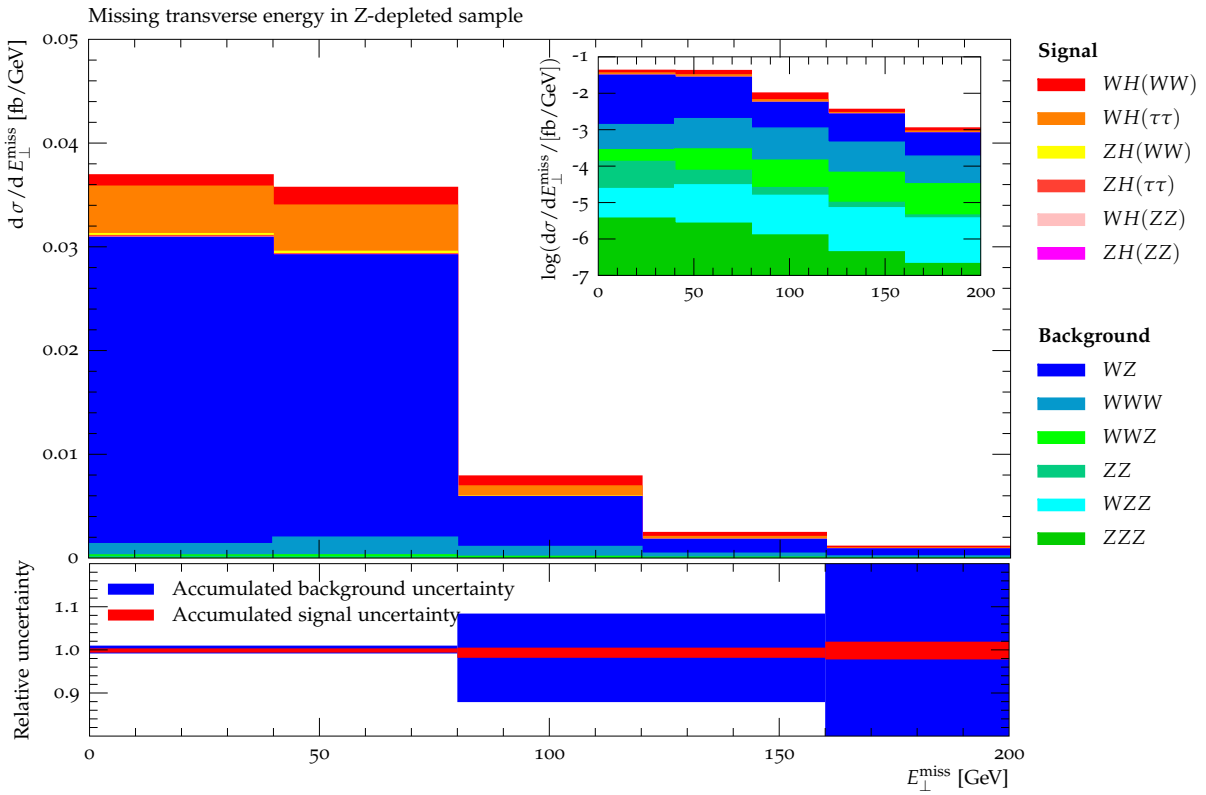

Figure 3: This shows the missing $E_\perp$ distribution for the signal and relevant backgrounds with the ATLAS cuts, which has a veto on any OSSF lepton pair.

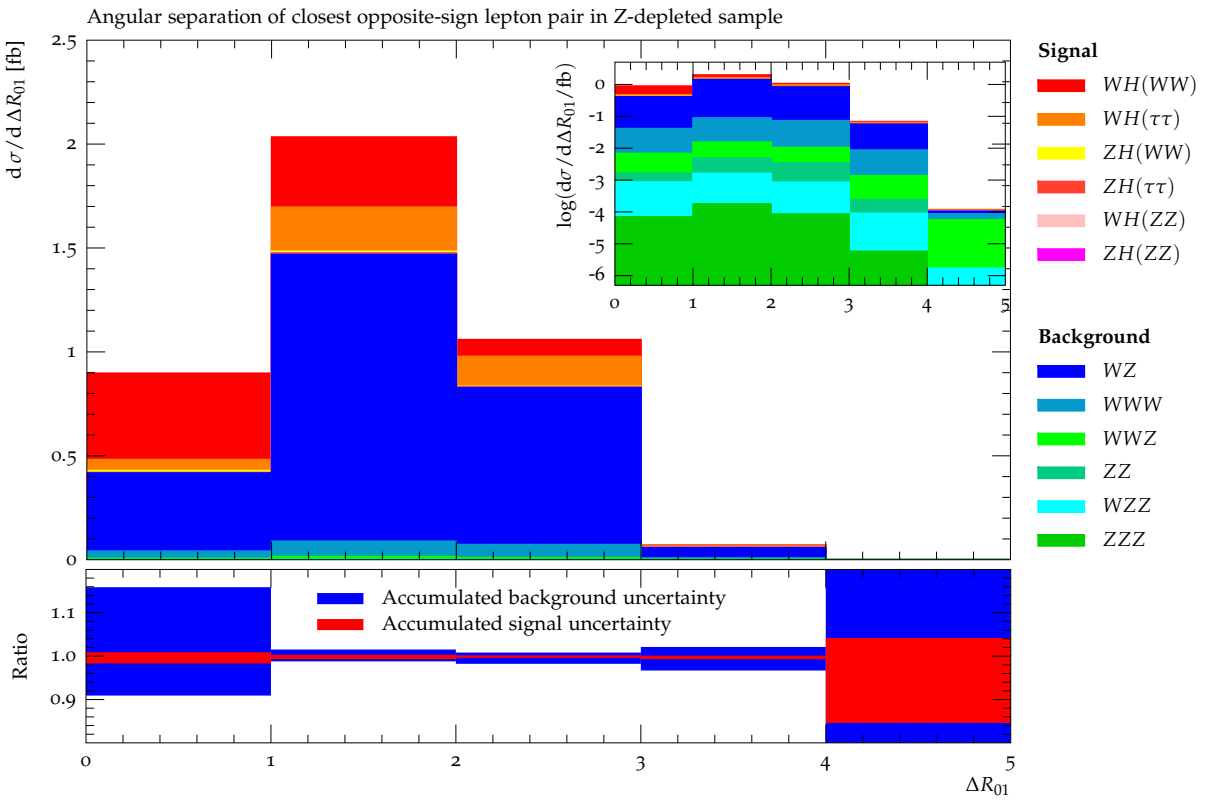

Figure 4: This shows the ΔR distribution of the closer pair of oppositely charged leptons in the case that no OSSF pair of leptons is found in the event with the ATLAS cuts.

malization and factorization scale variation with a typical effect on the few–percent level up to about 10% for some of the rare processes. In regions dominated by jet activity of course the MENLOPS samples, being at leading order accuracy, exhibit a stronger dependence than those processes simulated with MEPS@NLO. In addition, it is worth stressing that effects due to hadronisation and the underlying event are practically irrelevant for the uncertainties in the simulation of the processes considered here. Their main effect is on the isolation efficiency of the leptons, but this of course does not change the shape of any distribution in a visible way. The only exception here is the missing transverse momentum distribution where the inclusion of the underlying event may yield variations of about 20% compared to the parton level.

4 Conclusions

In this publication results for NLO QCD accurate predictions for multiple weak boson production were presented, and their application to trilepton final state analyses searching for effects of the Higgs boson has been highlighted. The calculation of the merged $W^{\pm}W^{+}W^{-}$ production is of particular importance as a complicated NLO process which is significant in all analyses based on trilepton final states, in particular where jet vetoes are being applied. We confirm, at NLO, that the relevant backgrounds to WH production are given by diboson and triboson production processes, if jet vetoes can be applied. We also show that the residual perturbative uncertainties in large fractions of the relevant phase space are of the order of 10% or even below. This will offer great opportunities for Higgs boson precision studies at the forthcoming LHC runs.

Acknowledgments

We are grateful to A. Denner, S. Dittmaier and L. Hofer for providing us with the one-loop tensor-integral library Collier.

This work has been supported in part by the European Commission through the "LHCPhenoNet" Initial Training Network PITN-GA-2010-264564, through the "MCnet" Initial Training Network PITN-GA-2012-315877, and through the "HiggsTools" Initial Training Network PITN-A-2012-316704. SH was supported by the U.S. Department of Energy under Contract No. DE–AC02–76SF00515. SP was supported by the SNSF. This research used resources of the National Energy Research Scientific Computing Center, which is supported by the Office of Science of the U.S. Department of Energy under Contract No. DE–AC02–05CH11231.

References

[1] G. Aad et al., ATLAS Collaboration collaboration, *Observation of a new particle in the search for the Standard Model Higgs boson with the ATLAS detector at the LHC*, Phys.Lett. **B716** (2012), 1–29, [arXiv:1207.7214 [hep-ex]].

[2] S. Chatrchyan et al., CMS Collaboration collaboration, *Observation of a new boson at a mass of 125 GeV with the CMS experiment at the LHC*, Phys.Lett. **B716** (2012), 30–61, [arXiv:1207.7235 [hep-ex]].

[3] F. Englert and R. Brout, *Broken Symmetry and the Mass of Gauge Vector Mesons*, Phys.Rev.Lett. **13** (1964), 321–323.

[4] P. W. Higgs, *Broken symmetries, massless particles and gauge fields*, Phys.Lett. **12** (1964), 132–133.

[5] P. W. Higgs, *Broken Symmetries and the Masses of Gauge Bosons*, Phys.Rev.Lett. **13** (1964), 508–509.

[6] G. Guralnik, C. Hagen and T. Kibble, *Global Conservation Laws and Massless Particles*, Phys.Rev.Lett. **13** (1964), 585–587.

[7] G. Aad et al., ATLAS Collaboration collaboration, *Measurement of the ZZ production cross section and limits on anomalous neutral triple gauge couplings in proton-proton collisions at sqrt(s) = 7 TeV with the ATLAS detector*, Phys.Rev.Lett. **108** (2012), 041804, [arXiv:1110.5016 [hep-ex]].

[8] G. Aad et al., ATLAS Collaboration collaboration, *Measurement of the WZ production cross section and limits on anomalous triple gauge couplings in proton-proton collisions at $\sqrt{s} = 7$ TeV with the ATLAS detector*, Phys.Lett. **B709** (2012), 341–357, [arXiv:1111.5570 [hep-ex]].

[9] G. Aad et al., ATLAS Collaboration collaboration, *Measurement of $W\gamma$ and $Z\gamma$ production cross sections in pp collisions at $\sqrt{s} = 7$ TeV and limits on anomalous triple gauge couplings with the ATLAS detector*, Phys.Lett. **B717** (2012), 49–69, [arXiv:1205.2531 [hep-ex]].

[10] S. Chatrchyan et al., CMS Collaboration collaboration, *Measurement of the $W\gamma$ and $Z\gamma$ inclusive cross sections in pp collisions at $\sqrt{s} = 7$ TeV and limits on anomalous triple gauge boson couplings*, arXiv:1308.6832 [hep-ex].

[11] ATLAS Collaboration collaboration, *Search for associated production of the Higgs boson in the $WH \to WWW^* \to \ell\nu\ell\nu\ell\nu$ and $ZH \to ZWW^* \to \ell\ell\ell\ell\nu\ell\nu$ channels with the ATLAS detector at the LHC.*

[12] CMS Collaboration collaboration, *VH with $H \to WW \to \ell\nu\ell\nu$ and $V \to jj$.*

[13] T. Han and S. Willenbrock, *QCD correction to the $pp \to WH$ and ZH total cross-sections*, Phys.Lett. **B273** (1991), 167–172.

[14] O. Brein, A. Djouadi and R. Harlander, *NNLO QCD corrections to the Higgs-strahlung processes at hadron colliders*, Phys.Lett. **B579** (2004), 149–156, [arXiv:hep-ph/0307206 [hep-ph]].

[15] G. Ferrera, M. Grazzini and F. Tramontano, *Associated WH production at hadron colliders: a fully exclusive QCD calculation at NNLO*, Phys.Rev.Lett. **107** (2011), 152003, [arXiv:1107.1164 [hep-ph]].

[16] A. Lazopoulos, K. Melnikov and F. Petriello, *QCD corrections to tri-boson production*, Phys.Rev. **D76** (2007), 014001, [arXiv:hep-ph/0703273 [hep-ph]].

[17] T. Binoth, G. Ossola, C. Papadopoulos and R. Pittau, *NLO QCD corrections to tri-boson production*, JHEP **0806** (2008), 082, [arXiv:0804.0350 [hep-ph]].

[18] V. Hankele and D. Zeppenfeld, *QCD corrections to hadronic WWZ production with leptonic decays*, Phys.Lett. **B661** (2008), 103–108, [arXiv:0712.3544 [hep-ph]].

[19] F. Campanario, V. Hankele, C. Oleari, S. Prestel and D. Zeppenfeld, *QCD corrections to charged triple vector boson production with leptonic decay*, Phys.Rev. **D78** (2008), 094012, [arXiv:0809.0790 [hep-ph]].

[20] K. Arnold, J. Bellm, G. Bozzi, M. Brieg, F. Campanario et al., *VBFNLO: A Parton Level Monte Carlo for Processes with Electroweak Bosons – Manual for Version 2.5.0*, arXiv:1107.4038 [hep-ph].

[21] F. Cascioli, P. Maierhöfer and S. Pozzorini, *Scattering Amplitudes with Open Loops*, Phys.Rev.Lett. **108** (2012), 111601, [arXiv:1111.5206 [hep-ph]].

[22] A. Denner, D. Dittmaier and L. Hofer, in preparation.

[23] A. Denner and S. Dittmaier, *Reduction of one-loop tensor 5-point integrals*, Nucl. Phys. **B658** (2003), 175–202, [hep-ph/0212259].

[24] A. Denner and S. Dittmaier, *Reduction schemes for one-loop tensor integrals*, Nucl. Phys. **B734** (2006), 62–115, [arXiv:hep-ph/0509141 [hep-ph]].

[25] A. Denner and S. Dittmaier, *Scalar one-loop 4-point integrals*, Nucl.Phys. **B844** (2011), 199–242, [arXiv:1005.2076 [hep-ph]].

[26] F. Krauss, R. Kuhn and G. Soff, *AMEGIC++ 1.0: A Matrix Element Generator In C++*, JHEP **02** (2002), 044, [hep-ph/0109036].

[27] T. Gleisberg and S. Höche, *Comix, a new matrix element generator*, JHEP **12** (2008), 039, [arXiv:0808.3674 [hep-ph]].

[28] S. Catani and M. H. Seymour, *A general algorithm for calculating jet cross sections in NLO QCD*, Nucl. Phys. **B485** (1997), 291–419, [hep-ph/9605323].

[29] S. Catani, S. Dittmaier, M. H. Seymour and Z. Trocsanyi, *The dipole formalism for next-to-leading order QCD calculations with massive partons*, Nucl. Phys. **B627** (2002), 189–265, [hep-ph/0201036].

[30] T. Gleisberg and F. Krauss, *Automating dipole subtraction for QCD NLO calculations*, Eur. Phys. J. **C53** (2008), 501–523, [arXiv:0709.2881 [hep-ph]].

[31] T. Gleisberg, S. Höche, F. Krauss, A. Schälicke, S. Schumann and J. Winter, *SHERPA 1.α, a proof-of-concept version*, JHEP **02** (2004), 056, [hep-ph/0311263].

[32] T. Gleisberg, S. Höche, F. Krauss, M. Schönherr, S. Schumann, F. Siegert and J. Winter, *Event generation with SHERPA 1.1*, JHEP **02** (2009), 007, [arXiv:0811.4622 [hep-ph]].

[33] S. Höche, F. Krauss, M. Schönherr and F. Siegert, *A critical appraisal of NLO+PS matching methods*, JHEP **09** (2012), 049, [arXiv:1111.1220 [hep-ph]].

[34] S. Höche, F. Krauss, M. Schönherr and F. Siegert, *W+n-jet predictions with MC@NLO in Sherpa*, Phys.Rev.Lett. **110** (2013), 052001, [arXiv:1201.5882 [hep-ph]].

[35] S. Frixione and B. R. Webber, *Matching NLO QCD computations and parton shower simulations*, JHEP **06** (2002), 029, [hep-ph/0204244].

[36] S. Frixione, P. Nason and B. R. Webber, *Matching NLO QCD and parton showers in heavy flavour production*, JHEP **08** (2003), 007, [hep-ph/0305252].

[37] Z. Nagy and D. E. Soper, *Matching parton showers to NLO computations*, JHEP **10** (2005), 024, [hep-ph/0503053].

[38] S. Schumann and F. Krauss, *A parton shower algorithm based on Catani-Seymour dipole factorisation*, JHEP **03** (2008), 038, [arXiv:0709.1027 [hep-ph]].

[39] F. Cascioli, P. Maierhöfer, N. Moretti, S. Pozzorini and F. Siegert, *NLO matching for $t\bar{t}b\bar{b}$ production with massive b-quarks*, arXiv:1309.5912 [hep-ph].

[40] T. Gehrmann, S. Höche, F. Krauss, M. Schönherr and F. Siegert, *NLO QCD matrix elements + parton showers in e^+e^- →hadrons*, JHEP **1301** (2013), 144, [arXiv:1207.5031 [hep-ph]].

[41] S. Höche, F. Krauss, M. Schönherr and F. Siegert, *QCD matrix elements + parton showers: The NLO case*, JHEP **1304** (2013), 027, [arXiv:1207.5030 [hep-ph]].

[42] S. Höche, J. Huang, G. Luisoni, M. Schönherr and J. Winter, *Zero and one jet combined NLO analysis of the top quark forward-backward asymmetry*, Phys.Rev. **D88** (2013), 014040, [arXiv:1306.2703 [hep-ph]].

[43] S. Höche, F. Krauss, P. Maierhöfer, S. Pozzorini, M. Schönherr et al., *Next-to-leading order QCD predictions for top-quark pair production with up to two jets merged with a parton shower*, arXiv:1402.6293 [hep-ph].

[44] F. Cascioli, S. Höche, F. Krauss, P. Maierhöfer, S. Pozzorini and F. Siegert, *Precise Higgs-background predictions: merging NLO QCD and squared quark-loop corrections to four-lepton + 0,1 jet production*, JHEP **1401** (2014), 046, [arXiv:1309.0500 [hep-ph]].

[45] P. Nason, *A new method for combining NLO QCD with shower Monte Carlo algorithms*, JHEP **11** (2004), 040, [hep-ph/0409146].

[46] S. Frixione, P. Nason and C. Oleari, *Matching NLO QCD computations with parton shower simulations: the POWHEG method*, JHEP **11** (2007), 070, [arXiv:0709.2092 [hep-ph]].

[47] S. Catani, F. Krauss, R. Kuhn and B. R. Webber, *QCD matrix elements + parton showers*, JHEP **11** (2001), 063, [hep-ph/0109231].

[48] L. Lönnblad, *Correcting the colour-dipole cascade model with fixed order matrix elements*, JHEP **05** (2002), 046, [hep-ph/0112284].

[49] F. Krauss, *Matrix elements and parton showers in hadronic interactions*, JHEP **0208** (2002), 015, [hep-ph/0205283].

[50] M. L. Mangano, M. Moretti and R. Pittau, *Multijet matrix elements and shower evolution in hadronic collisions: $Wb\bar{b} + n$-jets as a case study*, Nucl. Phys. **B632** (2002), 343–362, [hep-ph/0108069].

[51] J. Alwall et al., *Comparative study of various algorithms for the merging of parton showers and matrix elements in hadronic collisions*, Eur. Phys. J. **C53** (2008), 473–500, [arXiv:0706.2569 [hep-ph]].

[52] K. Hamilton, P. Richardson and J. Tully, *A modified CKKW matrix element merging approach to angular-ordered parton showers*, JHEP **11** (2009), 038, [arXiv:0905.3072 [hep-ph]].

[53] S. Höche, F. Krauss, S. Schumann and F. Siegert, *QCD matrix elements and truncated showers*, JHEP **05** (2009), 053, [arXiv:0903.1219 [hep-ph]].

[54] L. Lönnblad and S. Prestel, *Merging Multi-leg NLO Matrix Elements with Parton Showers*, JHEP **1303** (2013), 166, [arXiv:1211.7278 [hep-ph]].

[55] R. Frederix and S. Frixione, *Merging meets matching in MC@NLO*, JHEP **1212** (2012), 061, [arXiv:1209.6215 [hep-ph]].

[56] S. Plätzer, *Controlling inclusive cross sections in parton shower + matrix element merging*, JHEP **1308** (2013), 114, [arXiv:1211.5467 [hep-ph]].

[57] S. Höche and M. Schönherr, *Uncertainties in next-to-leading order plus parton shower matched simulations of inclusive jet and dijet production*, Phys.Rev. **D86** (2012), 094042, [arXiv:1208.2815 [hep-ph]].

[58] K. Hamilton and P. Nason, *Improving NLO-parton shower matched simulations with higher order matrix elements*, JHEP **06** (2010), 039, [arXiv:1004.1764 [hep-ph]].

[59] S. Höche, F. Krauss, M. Schönherr and F. Siegert, *NLO matrix elements and truncated showers*, JHEP **08** (2011), 123, [arXiv:1009.1127 [hep-ph]].

[60] *Search for the Associated Higgs Boson Production in the WH WWW() lll Decay Mode Using 4.7 fb1of Data Collected with the ATLAS Detector at s = 7 TeV*, Tech. Report ATLAS-CONF-2012-078, CERN, Geneva, Jul 2012.

[61] M. Cacciari, G. P. Salam and G. Soyez, *The Anti-k(t) jet clustering algorithm*, JHEP **0804** (2008), 063, [arXiv:0802.1189 [hep-ph]].

[62] M. Cacciari, G. P. Salam and G. Soyez, *FastJet user manual*, Eur.Phys.J. **C72** (2012), 1896, [arXiv:1111.6097 [hep-ph]].